

Accepted April 6th 2021

PARAMETRIC ANALYSIS AND MINIMIZATION OF ENTROPY GENERATION IN BIOINSPIRED MAGNETIZED NON-NEWTONIAN NANOFLUID PUMPING USING ARTIFICIAL NEURAL NETWORKS AND PARTICLE SWARM OPTIMIZATION

M. A. Abbas¹, O. Anwar Bég², A. Zeeshan³, Aatef Hobiny⁴, M. M. Bhatti^{5,*}

¹Department of Mathematics University of Baltistan Skardu, Gilgit Baltistan 16100, **Pakistan.**

²Professor and Director - Multi-Physical Engineering Sciences Group (MPESG), Aeronautical and Mechanical Engineering, School of Science, Engineering and Environment (SEE), The Crescent, Salford, M54WT, **UK.**

³Department of Mathematics, International Islamic University Islamabad, **Pakistan.**

⁴Nonlinear Analysis and Applied Mathematics (NAAM)-Research Group, Department of Mathematics, Faculty of Science, King Abdulaziz University, P.O. Box 80203, Jeddah 21589, **Saudi Arabia.**

⁵College of Mathematics and Systems Science, Shandong University of Science and Technology, Qingdao, Shandong, 266590, **China.** (mmbhatti@sdust.edu.cn)

ABSTRACT: Magneto-hydrodynamic rheological bio-inspired pumping systems are finding new applications in modern energy systems. These systems combined the electrically conducting properties of flowing liquids with rheological behaviour, biological geometries and propulsion mechanisms. Further enhancements in transport characteristics can be achieved with the deployment of nanofluids. Second law thermodynamic analysis also provides a useful technique for optimizing thermal performance by minimizing entropy generation. In the present study, all these aspects are combined to analyze the heat transfer in magnetic viscoelastic nanofluid flow in a two-dimensional deformable channel containing a rigid porous matrix under peristaltic waves subject to a transverse magnetic field. The Williamson model is deployed for the nanofluid rheology and the Buongiorno model for nanoscale effects. Under lubrication approximations, the conservation equations for mass, momentum, energy and nanoparticle species are simplified. These partial differential equations are further non-dimensionalized using relevant transformation variables. The mathematical model is solved analytically by means of the Homotopy Analysis Method (HAM). Next, entropy generation is minimized by applying Particle Swarm Optimization (PSO) and Artificial Neural Networks (ANN). In the first phase, the equation for Entropy generation is derived as a function of temperature distribution, velocity profile utilizing geometrical and thermophysical parameters. The first step is to discover entropy generation to estimate some extraordinary influencing parameters. In the next step, some specific multi-layer perceptron ANNs are trained, which depend on the information from the first stage. In the last step, PSO in the considered peristaltic flow is used to minimize entropy generation. The optimized value (minimum) of entropy generation is 3.65 kJ/kg acquired at magnetic parameter (M) = 3, Brownian motion parameter (N_b) = 0.3, thermophoresis parameter (N_t) = 0.5 and Brinkman number (B_r) = 2. Entropy generation is also very sensitive to both iteration number and magnetic field exhibiting a nonlinear topology.

KEY WORDS: *Magneto-hydrodynamic (MHD) energy systems; ANN; Entropy Generation; Bio-inspired nano-energy systems.*

1. INTRODUCTION:

In recent decades, numerous studies have considered the use of the second law of thermodynamics in optimizing thermal engineering systems. Entropy generation minimization has become a critical component of heat transfer simulations and mobilized considered computational and analytical activity in many branches of engineering sciences including rotating power generation, coating systems, heat ducts, renewable energy and microscale/nanoscale thermophysics. These studies have amalgamated many branches of fluid dynamics and thermosciences including slip hydrodynamics, rheology, magnetohydrodynamics, thermal convection, conduction and radiative heat transfer. Arikoglu *et al.* [1] investigated the impact of Joule and slip on entropy generation in the hydromagnetic flow over a solitary spinning plate using the semi-numerical differential transform method. Rashidi *et al.* [2] conducted first and the second law thermodynamic analysis of electrically conducting flow from a spinning disk under a uniform vertical magnetic field. They also employed Artificial Neural Network (ANN) and Particle Swarm Optimization (PSO) methods to compute limits for entropy generation. Ramana Murthy *et al.* [3] employed Bejan's entropy minimization method to study the radiative, conductive and convective heat transfer optimization in couple stress non-Newtonian duct flows. Tarlet *et al.* [4] performed a first and second law thermodynamic optimization for a cylinder heat exchanger outfitted with multi-scale distributor. The entropy generation in nanofluid flow from a porous extending surface was explored by Sheikholeslami *et al.* [5], who showed that an increment in nanoparticle volume fraction diminishes entropy generation ratio. Specialists employ the second law of thermodynamics to acquire ideal heat organization structure by minimizing irreversibility, which can improve the effectiveness of mechanical frameworks. This approach was pioneered by American engineer, Bejan [6]. The work of entropy generation is a proportion of the available irreversibility dimension in a process. Production of entropy generation involves irreversibility in thermodynamics, for instance, convective heat exchange characteristics, heat exchange across restricted temperature corners, dense scattering effects and magnetic field effects that can in industrial process e.g. magnetic rheological materials processing [7]. Compared with the conventional first law of thermodynamics (energy conservation), the second law of thermodynamics is more dependable, since it permits the optimization of efficiency in thermal engineering systems to be robustly achieved [8]. Entropy generation analysis has also been applied by Afridi and Qasim [9] in radiative-convective boundary layer flow from a thin needle. Nonlinear radiative magneto-convective slip nanofluid flow with entropy production in a vertical permeable microchannel has been investigated by Lopez *et al.* [10] for water-aluminum oxide, who showed that entropy generation is depleted with wall suction and nanoparticle fraction. Baag *et al.* [11] examined analytically the irreversibility in the hydromagnetic convection flow of viscoelastic fluid from a stretching sheet embedded in a permeable material with Darcy's law using Kummer mathematical functions. Liu *et al.* [12] investigated analytically the entropy generation in electromagnetic flow in a curved microchannel. They observed that local entropy generation decays from the boundary to the core region whereas entropy generation rate is elevated with

Brinkman (viscous heating) number and Hartmann magnetic number. Similarly numerical simulation has been carried out to examine the thermal characteristics and second law analysis of turbulent model of nanofluid by Nakhchi, M. E., & Rahmati, M. T [13]. The same author discussed Numerical investigation of heat transfer enhancement inside heat exchanger tubes fitted with perforated hollow cylinders and perforated louvered strip inserts [14-15].

In many modern thermal power processes, magnetic fields are being exploited to enhance efficiency, control and also by-pass heat recycling. Magnetic field can be utilized to modify entropy generation and manipulate the rate of heat exchange [16]. For thermal optimization, engineers utilize the second law of thermodynamics to decrease the irreversibility and the entropy generation, and this can greatly enhance effectiveness of modern technologies [17]. In recent years, significant progress has also been made in thermodynamics and heat transfer using artificial neural networks (ANNs) and genetic algorithms (GAs). Kalogirou [18] has connected Artificial Intelligence (AI) methods to demonstrate control and execution of combustion processes. DehKiani *et al.* [19] deployed ANN for optimized exhaust emissions (carbon monoxide, nitrogen oxide etc) in a spark ignition engine. Mohandes and Gandhidasan [20] employed an ANN-based model for simulating the connection between the outlet parameters of a lithium chloride randomly packed dehumidifier with desiccant channel. They deployed 8 parameters as inputs to the ANN, namely: air and desiccant flow rates, air and desiccant inlet temperatures, air inlet humidity, desiccant inlet concentration, dimensionless temperature ratio, and inlet temperature of the cooling water. Smrekar *et al.* [21] utilized ANN models with real plant information to forecast the new steam properties from a brown coal-fired boiler of a Slovenian electricity plant. Atashkari *et al.* [22] implemented a Multi Objective Genetic Algorithm (MOGA) for enhancement of thermodynamic performance of turbojet motors. Mohagheghi and Shayegan [23] determined an ideal thermodynamic exhibition condition for heat recovery steam generators utilizing a Genetic Algorithm (GA). ANN based models had been increasingly used in recent years. Rashidi *et al.* [24] applied a combined GA and ANN approach for trans-critical thermodynamic cycles, using heat effectiveness and energy productivity as target capacities for parametric enhancement. Rao and Patel [25] used a Particle swarm optimization (PSO) i.e. population based stochastic optimization technique for thermodynamic analysis of a cross stream plate-balance heat converter. Other investigations include Rashidi *et al.* [26] on parametric appraisal and progress of regenerative Claudius and basic Rankine cycles with two feed-water radiators using an artificial bees' colony (ABC) and artificial neural network (ANN) using energy productivity and heat capability as target functions. Zhang *et al.* [27] investigated wastewater plant pump performance employing a neural network algorithm for pump energy consumption and fluid flow rate in addition to a scheduling model and particle swarm optimization algorithm. All these studies have demonstrated the excellent capability of neural networks and genetic algorithms in modern thermal engineering.

A further important development in modern thermal and industrial engineering designs has been the use of *bio-inspired* concepts. This approach embraces fluid dynamics, geometric configurations, transport mechanisms and many other biomimetic phenomena. Recent examples

include biological hydrogels for human-interfacable electronics [28], fish-inspired piezoelectric energy harvesters [29], bio-shape memory materials [30] and bio-slip designs for energy generation [31]. A very efficient propulsion mechanism deployed both internally in animal and plant physiology and externally in locomotion (e.g. snakes) is *peristalsis* [32]. This utilizes the rhythmic expansion and contraction of surface waves to achieve very effective and also tunable transport and features in for example, intestinal dynamics, blood flows, phloem translocation in trees, bat wing control, earthworm movement etc. Peristaltic pumps do not require the high maintenance costs of conventional industrial designs and furthermore feature a minimum number of working parts. They also mitigate reflux and backflow or leakage problems for hazardous or corrosive liquids. Peristalsis-inspired nanofluid pumps with electrical field control have been recently studied by Narla *et al.* [33]. Further studies include Bhatti *et al.* [34] (on electrical and magnetic field effects in radiative dusty flows), Bhatti *et al.* [35] (coagulation in two-phase peristaltic endoscopic annular flows), Ali *et al.* [36] (electrokinetic pumping in microfluidics), Tripathi *et al.* [37] (finite length capillary electro-osmotic blood flows), Abdelsalam *et al.* [38] (combined cilia-generated and peristaltic magnetic double diffusive pumping) and Prakash *et al.* [39] (hybrid electro-nanofluid transport under peristaltic waves).

Many modern energy systems are also featuring porous media. These fibrous materials can be customized to enhance thermal storage and efficiencies. At low Reynolds numbers the Darcy law is deployed for modelling such systems (viscous dominated regime). Although porous media are very complex due to random distribution of solid fibers and voids, often engineers can approximate their transport characteristics by assuming isotropic behaviour i.e. a single permeability is assumed in all directions. Recent works featuring porous media include Weng *et al.* [40] (metal foam-based fuel cells), Alkam and Al-Nimr [41] (hybrid porous media solar collector pipes), El Tawil and Kamel [42] (magnetohydrodynamic random flows in fuel cells), Kamel [43] (nuclear heat transfer control with porous media damping) and Zueco *et al.* [44] (two-phase hydromagnetic flows in permeable materials for materials processing) and Bég *et al.* [45] (geothermal energy plumes). These studies have featured both Newtonian and non-Newtonian (rheological) fluid models. Non-Newtonian flows arise for example in doping working fluids with high-polymer additives to enhance flow and minimize drag. Mathematical models of rheological fluids are therefore extremely useful in simulating modern energy and bio/chemical engineering systems [46] and include pseudoplastic power-law models [47]. An alternate model is the viscoelastic Williamson model [48] which quite accurately models numerous energetic fluent media, certain polymers, microgel-free xanthan polysaccharide dissolved in salt water [49] etc. This model has been used successfully in recent years by Hayat [50] and Bég *et al.* [51] in peristaltic pumping fluid mechanics.

In the current work, motivated by optimizing bio-inspired thermal energy systems, we study theoretically and computationally the entropy generation in magnetohydrodynamic radiative double diffusive peristaltic pumping of nanofluids in an energy duct containing a porous medium saturated with Williamson non-Newtonian fluid. Chemical reaction and heat source effects are also considered. Due to the complexity of the equations and the multiplicity of the parameters, the

optimization process is executed using ANN and PSO. For this purpose, entropy generation is selected as the objective function. The mathematical flow model is transformed with appropriate dimensionless variables and solved as a boundary value problem with the powerful homotopy analysis method (HAM) [52]. Several researchers used these powerful techniques to solve the highly nonlinear equations [53-57]. For minimizing rate of the entropy generation, the effective parameters, namely, Hartmann (magnetic) number, thermophoresis, Brownian motion parameter and Brinkman (dissipation) number are investigated and optimized. The results obtained provide an improved perspective for diminishing the irreversibility causes. The mathematical formulation is developed in section 2 and the homotopy solutions elaborated in section 3. Section four describes the optimization procedure for the minimization of entropy generation. Section 5 provides the result visualization and discussion. Finally concluding remarks and future pathways for extension of the current study are given.

2. MATHEMATICAL MODEL

Peristaltic motion of an electroconductive incompressible reactive nanofluid through a two-dimensional channel (energy duct) containing a non-deformable, sparsely packed, high permeability porous medium, with sinusoidal wave propagation at the walls, is considered. Radiative heat flux, heat generation, thermal and species buoyancy are also present. As visualized in **Fig. 1**, a Cartesian coordinate system is adopted in which the ξ axis is orientated along the center line (in the direction of wave generation) and the η axis is transverse to it. B_0 is a uniform, static external magnetic field is imposed transverse to the deformable channel length. The porous medium achieves better thermal conduction in the propulsion and also allows flow control of peristaltic propulsion waves. The wall geometry is simulated via the following equations [38-39]:

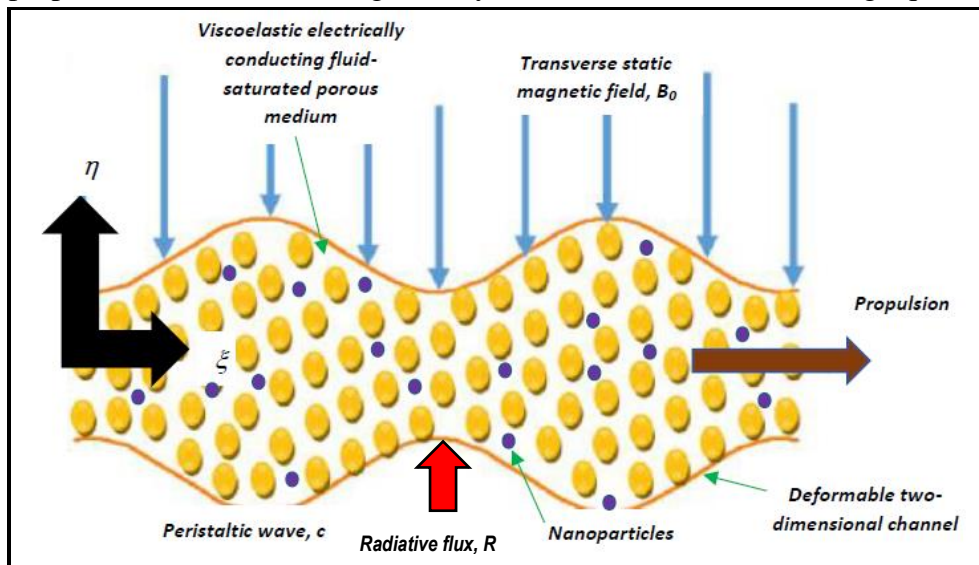


Fig. 1: Physical model for bioinspired magnetohydrodynamic nanofluid channel

$$\xi_h = \alpha(\xi) + l \sin k\omega, \quad k = \frac{2\pi}{\lambda}, \quad \omega = \xi - w_c t, \quad \alpha(\xi) = \alpha_0 + \alpha_n \xi, \quad (1)$$

Here $\alpha(\xi)$ denotes the width of the channel, l is the amplitude of the wave, w_c the wave speed, t the time, α_0 the half width from the inlet, and α_n is a constant. The governing equations are:

Mass conservation (continuity):

$$\frac{\partial \bar{u}}{\partial \xi} + \frac{\partial \bar{v}}{\partial \eta} = 0, \quad (2)$$

Axial Momentum conservation:

$$\begin{aligned} \rho_d \left(\frac{\partial \bar{u}}{\partial t} + \bar{u} \frac{\partial \bar{u}}{\partial \xi} + \bar{v} \frac{\partial \bar{u}}{\partial \eta} \right) = & -\frac{\partial p}{\partial \xi} + \frac{\partial}{\partial \xi} \chi_{\xi\xi} + \frac{\partial}{\partial \eta} \chi_{\xi\eta} - \sigma B_0^2 \bar{u} - \frac{\mu}{k} \bar{u} \\ & + g \left[(1-C) \rho_d \zeta (T - T_0) - (\rho_p - \rho_d)(C - C_0) \right], \end{aligned} \quad (3)$$

Transverse Momentum conservation:

$$\begin{aligned} \rho_d \left(\frac{\partial \bar{v}}{\partial t} + \bar{u} \frac{\partial \bar{v}}{\partial \xi} + \bar{v} \frac{\partial \bar{v}}{\partial \eta} \right) = & -\frac{\partial p}{\partial \eta} + \frac{\partial}{\partial \xi} \chi_{\eta\xi} + \frac{\partial}{\partial \eta} \chi_{\eta\eta} \\ & + g \left[(1-\bar{C}) \rho_d \zeta (\bar{T} - \bar{T}_0) - (\rho_p - \rho_d)(\bar{C} - \bar{C}_0) \right], \end{aligned} \quad (4)$$

Energy conservation:

$$\begin{aligned} (\rho c)_d \left(\frac{\partial \bar{T}}{\partial t} + \bar{u} \frac{\partial \bar{T}}{\partial \xi} + \bar{v} \frac{\partial \bar{T}}{\partial \eta} \right) = & k_t \left(\frac{\partial^2 \bar{T}}{\partial \xi^2} + \frac{\partial^2 \bar{T}}{\partial \eta^2} \right) - \frac{\partial R}{\partial \eta} + H_0 \\ & + (\rho c)_p \left[\bar{D}_B \left(\frac{\partial \bar{T}}{\partial \xi} \frac{\partial \bar{C}}{\partial \xi} + \frac{\partial \bar{T}}{\partial \eta} \frac{\partial \bar{C}}{\partial \eta} \right) + \bar{D}_{\bar{T}} \left(\frac{\partial \bar{T}}{\partial \eta} \right) \right], \end{aligned} \quad (5)$$

Nanoparticle species conservation:

$$\left(\frac{\partial \bar{C}}{\partial t} + \bar{u} \frac{\partial \bar{C}}{\partial \xi} + \bar{v} \frac{\partial \bar{C}}{\partial \eta} \right) = \bar{D}_B \left(\frac{\partial^2 \bar{C}}{\partial \xi^2} + \frac{\partial^2 \bar{C}}{\partial \eta^2} \right) + \frac{\bar{D}_{\bar{T}}}{\bar{T}_0} \left(\frac{\partial^2 \bar{T}}{\partial \xi^2} + \frac{\partial^2 \bar{T}}{\partial \eta^2} \right) - C_k (\bar{C} - \bar{C}_0), \quad (6)$$

Here ρ_d denotes the density, p the pressure, σ the electrical conductivity, μ the viscosity, k the permeability of the porous medium, ρ_p the nanoparticle density, k_t the thermal conductivity, \bar{T} the temperature, \bar{C} the concentration, $(\rho c)_p$ the effective heat capacity of nanoparticle, \bar{D}_B the mass diffusivity coefficient, $\bar{D}_{\bar{T}}$ the coefficient of thermophoretic diffusion, C_k the chemical reaction, H_0 the heat source, $(\rho c)_d$ the heat capacity of fluid, ζ the volumetric expansion coefficient of the fluid, g the gravity, and R the radiation parameter. The extra stress tensor for

Williamson fluid [47, 48] is defined as:

$$\chi = [\mu_\infty + (\mu_0 + \mu_\infty)(1 - \tau\Lambda)^{-1}]A_1, \quad (7)$$

We have considered $\mu_\infty = 0$ and $\tau\Lambda < 1$. Here:

$$\tau = \sqrt{\frac{\text{trac}(A_1^2)}{2}}, A_1 = \text{grad } \mathbf{V} + [\text{grad } \mathbf{V}]^T. \quad (8)$$

The following non-dimensional quantities are defined:

$$\begin{aligned} \tilde{\xi} &= \frac{\xi}{\lambda}, \tilde{\eta} = \frac{\eta}{\alpha_0}, v = \frac{\bar{v}}{w_c \delta}, \tilde{p} = \frac{p\alpha_0^2}{\lambda w_c \mu}, \tilde{\xi}_h = \frac{\xi_h}{\alpha_0}, \\ \text{Re} &= \frac{w_c \rho_d l}{\mu}, \delta = \frac{l}{\lambda}, \theta = \frac{\bar{T} - \bar{T}_0}{\bar{T}_1 - \bar{T}_0}, \Theta = \frac{\bar{C} - \bar{C}_0}{\bar{C}_1 - \bar{C}_0}, \end{aligned} \quad (9)$$

Implicit in the present study are low Reynolds number and long wavelength approximations for which the current problem assumes creeping flow. By using dimensionless quantities in Eqn. (9), we get the subsequent equations (ignoring the tilde):

$$\frac{\partial^2 u}{\partial \eta^2} + We \frac{\partial}{\partial \eta} \left(\frac{\partial u}{\partial \eta} \right)^2 - \frac{u}{k} - M^2 u - Gr_F \Theta + Gr_T \theta = \frac{dp}{d\xi}, \quad (10)$$

$$\left(\frac{1}{\text{Pr}} + R_n \right) \frac{\partial^2 \theta}{\partial \eta^2} + N_t \left(\frac{\partial \theta}{\partial \eta} \right)^2 + \beta + N_b \frac{\partial \theta}{\partial \eta} \frac{\partial \Theta}{\partial \eta} = 0, \quad (11)$$

$$\frac{\partial^2 \Theta}{\partial \eta^2} + \frac{N_t}{N_b} \frac{\partial^2 \theta}{\partial \eta^2} - \gamma \Theta = 0, \quad (12)$$

Here Weissenberg number is denoted by We while k is the permeability, M the Hartmann number, Gr_F and Gr_T the basic-density (nanoparticle species) Grashof number and the thermal Grashof number, respectively. Further, the Prandtl number and radiation parameter are denoted by Pr and R_n respectively, ϕ is the peristaltic wave amplitude ratio, N_b and N_t the Brownian motion and the thermophoresis parameter, γ is a first order chemical reaction parameter and β is the heat source parameter. These parameters are defined as follows:

$$\begin{aligned} Gr_F &= \frac{g\alpha_0^3 (\rho_p - \rho_d) (\bar{C} - \bar{C}_0)}{\rho_p \nu^2}, \tilde{k} = \frac{k}{\mu}, M = \sqrt{\frac{\sigma}{\mu}} \alpha_0 B_0, We = \frac{\Lambda w_c}{\alpha_0}, \tau = \frac{\tau \alpha_0}{w_c}, \text{Pr} = \frac{\nu (\rho c)_d}{k_t}, \\ Gr_T &= \frac{g\alpha_0^3 (1 - \bar{C}) \rho_d \zeta (\bar{T} - \bar{T}_0)}{\rho_p \nu^2}, N_b = \frac{(\rho c)_p \bar{D}_B (\bar{C}_1 - \bar{C}_0)}{k_t}, N_t = \frac{(\rho c)_p \bar{D}_T (\bar{T}_1 - \bar{T}_0)}{\bar{T}_0}, \\ \gamma &= \frac{C_k \alpha_0^2}{\nu}, R_n = \frac{16 \tilde{\sigma} \bar{T}_0^3}{3 \hat{k} \mu c_f}, \beta = \frac{H_0 \alpha_0^2}{(\bar{T}_1 - \bar{T}_0) \nu c_p}, \phi = \frac{l}{\alpha_0}, \end{aligned} \quad (13)$$

The dimensionless associated boundary conditions emerge as:

$$\Theta(0) = \theta(0) = \frac{\partial u}{\partial \eta}(0) = 0, \quad (14)$$

$$\Theta(\xi_h) = \theta(\xi_h) = 1, u(\xi_h) = 0, \quad (15)$$

With magnetic field, the entropy generation can be determined from an entropy balance for the heat and mass exchange as follows:

$$\begin{aligned} S_{\text{gen}} = & \frac{k_t}{\bar{T}_0^2} \left[1 - \frac{\partial R}{\partial \eta} \right] (\nabla \bar{T})^2 + \frac{\mu}{\bar{T}_0} \chi_{\xi\eta} \left(\frac{\partial \bar{u}}{\partial \eta} \right) + \left(\frac{\sigma B_0^2}{\bar{T}_0} + \frac{\mu}{\bar{T}_0 k} \right) \bar{u}^2 \\ & + \frac{R \bar{D}_B}{\bar{C}_0} (\nabla \bar{C})^2 + \frac{R \bar{D}_B}{\bar{T}_0} \nabla \bar{C} \cdot \nabla \bar{T}. \end{aligned} \quad (16)$$

The dimensionless form of entropy generation reads as:

$$\begin{aligned} \text{Ns} = & [1 + R_n] \left(\frac{\partial \theta}{\partial \eta} \right)^2 + \frac{B_r}{\Omega} \left(\frac{\partial \bar{u}}{\partial \eta} \right) \left(\frac{\partial \bar{u}}{\partial \eta} + We \left(\frac{\partial \bar{u}}{\partial \eta} \right)^2 \right) \\ & + \frac{B_r}{\Omega} \left(\frac{1}{k} + M^2 \right) \bar{u}^2 + \Gamma \left(\frac{\Upsilon}{\Omega} \right)^2 \left(\frac{\partial \Theta}{\partial \eta} \right)^2 + \zeta \frac{\partial \Theta}{\partial \eta} \frac{\partial \theta}{\partial \eta}. \end{aligned} \quad (17)$$

Here the dimensionless temperature difference, diffusive coefficient, concentration difference, constant parameter, and Brinkman number, are represented as:

$$\begin{aligned} S_g = & \frac{k_t (\bar{T}_1 - \bar{T}_0)^2}{\bar{T}_0^2 b_0^2}, B_r = \frac{\mu c^2}{k_t (\bar{T}_1 - \bar{T}_0)}, \zeta = \frac{R \bar{D}_B \bar{T}_0 (\bar{C}_1 - \bar{C}_0)}{k_t (\bar{T}_1 - \bar{T}_0)}, \\ \Omega = & \frac{(\bar{T}_1 - \bar{T}_0)}{\bar{T}_0}, \Gamma = \frac{R \bar{D}_B \bar{C}_0}{k_t}, \Upsilon = \frac{(\bar{C}_1 - \bar{C}_0)}{\bar{C}_0}, \end{aligned} \quad (18)$$

3. HOMOTOPY SOLUTIONS OF BOUNDARY VALUE PROBLEM

The emerging boundary value problem i.e. Eqns. (10)-(12) under conditions (14, 15) is nonlinear and strongly coupled. Many numerical methods are available for solving such a system. However here we implement the popular homotopy analysis method (HAM) developed by Liao [58]. This method has been extensively deployed in non-Newtonian magnetohydrodynamics [59] and nanofluid mechanics [60]. Considering Eqn. (10) to Eqn. (12) and solving using HAM the n^{th} order deformation equation takes the form:

$$\left. \begin{aligned} (1-q)L_1[u(\eta, q) - u_0(\eta)] &= q\hbar_1 N_1[u(\eta, q), \theta(\eta, q), \Theta(\eta, q)], \\ (1-q)L_2[\theta(\eta, q) - \theta_0(\eta)] &= q\hbar_2 N_2[u(\eta, q), \theta(\eta, q), \Theta(\eta, q)], \\ (1-q)L_3[\phi(\eta, q) - \phi_0(\eta)] &= q\hbar_3 N_3[u(\eta, q), \theta(\eta, q), \Theta(\eta, q)]. \end{aligned} \right\} \quad (19)$$

To achieve an analytical solution, the following initial approximations $u_0(\eta), \theta_0(\eta), \Theta_0(\eta)$ are used:

$$u_0 = \frac{\cosh N^2 \eta - \cosh N^2 h}{\cosh N^2 h}, \theta_0 = \Theta_0 = \frac{\eta}{h} \quad (20)$$

Here the supplementary linear operators L_1 for velocity and L_2 for temperature and nanoparticle concentration profiles are:

$$L_1 = \frac{\partial^2}{\partial \eta^2} - \frac{1}{k} - M^2, L_2 = \frac{\partial^2}{\partial \eta^2}, \quad (21)$$

Finally, the nonlinear operators N_1 , N_2 and N_3 for velocity, temperature and nanoparticle concentration are written according to Eqns. (21) - (19) as:

$$N_1 \left[u(\eta, \bar{\xi}), \theta(\eta, \bar{\xi}), \Theta(\eta, \bar{\xi}) \right] = -\frac{\partial p}{\partial x} + \frac{\partial^2 u(\eta, \bar{\xi})}{\partial y^2} + We \frac{\partial}{\partial y} \left(\frac{\partial u(\eta, \bar{\xi})}{\partial y} \right)^2 - M^2 u(\eta, \bar{\xi}) - \frac{u(\eta, \bar{\xi})}{k} - Gr_F \Theta(\eta, \bar{\xi}) + Gr_T \theta(\eta, \bar{\xi}), \quad (22)$$

$$N_2 \left[u(y, \xi), \theta(y, \xi), \Theta(y, \xi) \right] = \left(\frac{1 + R_n}{Pr} \right) \frac{\partial^2 \theta(y, \xi)}{\partial y^2} + N_t \left(\frac{\partial \theta(y, \xi)}{\partial y} \right)^2 + \beta + N_b \left(\frac{\partial \theta(y, \xi)}{\partial y} \right) \left(\frac{\partial \Theta(y, \xi)}{\partial y} \right), \quad (23)$$

$$N_3 \left[u(y, \xi), \theta(y, \xi), \Theta(y, \xi) \right] = \frac{\partial^2 \Theta(y, \xi)}{\partial y^2} - \gamma \Theta(y, \xi) + \frac{N_t}{N_b} \frac{\partial^2 \theta(y, \xi)}{\partial y^2}. \quad (24)$$

Defining the following expansions:

$$\left. \begin{aligned} u(\eta, q) &= u_0(\eta) + \sum_{k=1}^n q^k u_k(\eta), \\ \theta(\eta, q) &= \theta_0(\eta) + \sum_{k=1}^n q^k \theta_k(\eta), \\ \Theta(\eta, q) &= \Theta_0(\eta) + \sum_{k=1}^n q^k \Theta_k(\eta), \end{aligned} \right\} \quad (25)$$

Utilizing the above expansions, $u_0(\eta), \theta_0(\eta), \Theta_0(\eta)$ as referenced in Eqn. (25) in Eqns. (19) generates an arrangement of direct differential equations with their significant limit conditions. The solution deforms from initial guesses to approximate values when q changes continuously from 0 to 1. Here \hbar is a convergence control parameter with values which are optimized to get the minimum “Residual Error” using an appropriate genetic algorithm. **Fig. 2** shows a flow chart visualizing the procedure followed in the optimization process.

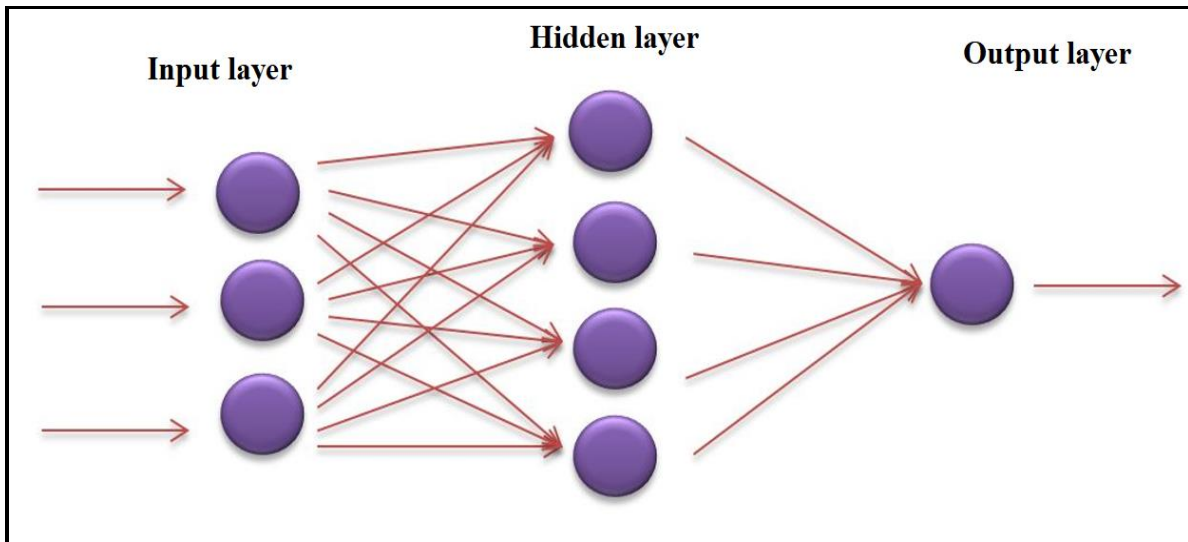


Figure 2: Schematic graph of regular Multi-Layer Feed Forward (MLFF) neural-organize design.

4. PARAMETRIC OPTIMIZATION TECHNIQUE

i. Artificial Neural Network (ANN).

The ANN relies upon an equivalent plan to an organismic mind. They are a sort of biological multi-processor system utilizing essential scalar messages and direct handling segments, and characterized by a high level of association and assenting connections between components. Multi-Layer Feed Forward (MLFF) is the most conspicuous sort of ANN (see Fig. 2). The framework generally connects a data layer (input), some concealed layers, a yield layer and also various affiliation loads within which data is secured. The route toward altering the association is weighted (biased) with a sensible learning methodology termed “training”. In the present investigation, an ANN is prepared dependent on a Back-Error Propagation (BEP) neural system for the estimation of entropy generation. The contribution of the referenced ANNs are different estimations of Brownian movement parameter, magnetic parameter, thermophoresis parameter and Brinkman number featured in the fluid dynamic model described in section 2. In the system, PURELIN and TANSIG refer to the transfer functions for *neurons of hidden layer* and the *output layers* respectively:

$$\mathcal{G}(\xi) = \frac{2}{-1 + (1 - e^{-2\xi})}, \mathcal{H}(\xi) = \xi, \quad (26)$$

The most extensively employed erudition procedure of the MLFF neural system is the BEP, a method proposed by McClelland and Rumelhart [61] in a seminal study conducted at the Massachusetts Institute of Technology (MIT) which focused on cognitive computing. In current work, the organization of the Multi-Layer Perceptron (MLP) neural framework includes three different layers, for example the information (input), the hidden layer and the output layers. The

sizes of the parameters A_{ab} are the weights allocated between the information and hidden layers, and those of A_{bc} are weights ascribed between the hidden layer and output layer. Different stages are required for a Back-Error Propagation (BEP) neural system. We used three different types of algorithms to train our data. While training we have to check the performance of the network for which we use a Mean Square Error (MSE). This shows the performance of the training graphically. Also, we analyze the designed networks by using regression and histograms of network errors. This technique has a better speculation property which is frequently used to linearize the equations. [62-63]. The Bayesian regularization technique employs the *Levenberg-Marquardt algorithm*. The Jacobian j_X is calculated by using back propagation and j_X demonstrates the exhibition concerning the weight and inclination factor X . We can adjust the variables to manage the Levenberg-Marquardt algorithm as follows:

$$J = j_X \times j_X, Je = j_X \times E, dX = -\frac{jj + I\mu}{Je} \quad (27)$$

The terms E and I are the error and the identity matrix respectively. The value of the parameter μ is increased by μ_{inc} and decreased by μ_{dec} . The procedure continues until the change appearing above produces a satisfactory value. To calculate the Jacobian j_X , the parameter μ_{red} is used which quantifies speed and memory utilization. The Levenberg-Marquardt algorithm runs the fastest compared with other algorithms; however, it can require a lot of memory only when ($\mu_{red} = 1$). Further, for the case when ($\mu_{red} > 1$), the memory required increases by a factor of two, yet eases back in the Levenberg-Marquardt algorithm to some degree i.e. for large values of μ_{red} , it keeps on diminishing the measure of memory required and increment in compilation times decays.

ii. Particle Swarm Optimization:

Particle Swarm Optimization (PSO) is an advanced system designed by Eberhart and Kennedy [64], inspired by biology such as the social behavior of fish schooling and bird herding. PSO [65] shares plentiful resemblances with developmental computation methods, for example, the Genetic Algorithm. The streamlining methodology of PSO commences with a population of arbitrary arrangements and scans for optimal arrangements by refreshing of generations. In contrast to GA, the PSO has no *advance operator*, such as crossover and mutation. In the PSO algorithm, a global *topology* is employed as the swarm communication structure and this topology allows all particles to communicate with all the other particles, thus the whole swarm share the same best position from a single particle. Every particle monitors its directions in the space of the issue related to the best arrangement (best fit) it has accomplished so far, named " P_{best} ". Another "best" esteem followed by the use of PSO is the best value that any object in the particle's neighborhood has acquired to date. The parameter is designated as " L_{best} ". At some point once an element accepts the whole population as its topological neighbor, a worldwide best, termed the " G_{best} ", is selected as the best value. The PSO idea at every time organizes comprises of changing every particle's speed in the direction of its " P_{best} " and " L_{best} " areas. Acceleration utilizing an irregular

span is biased by isolated arbitrary figures being produced for increasing velocity towards " L_{best} " and " P_{best} " location. A demonstration of PSO methodology is depicted in **Fig. 3**.

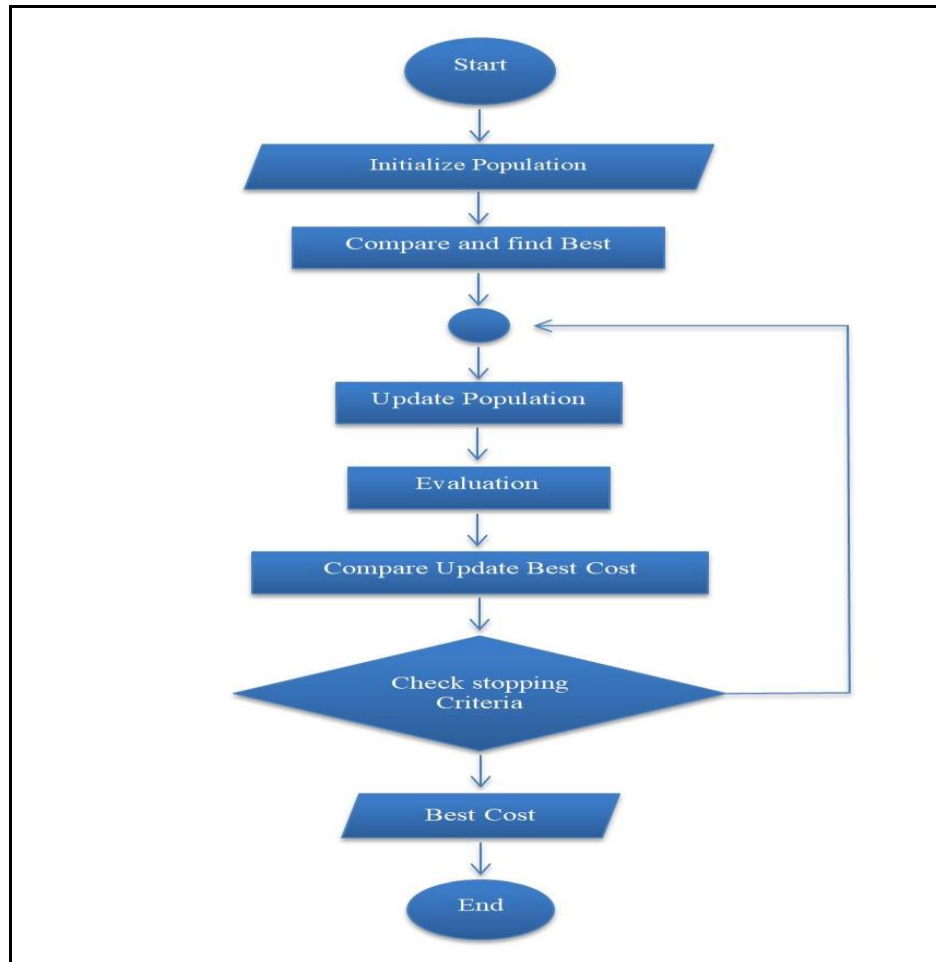


Figure 3: Flowchart of the PSO.

PSO is a progression framework which wards on populations shaped by the original Eberhart-Kennedy algorithm [66], which was based on motivations by communal conduct of fish coaching or round up of birds. PSO shares various similarities with formative calculation techniques, for instance, Genetic Algorithms. The streamlining strategy of PSO is initiated with the populace of arbitrary plans and achieves an ideal scenario by stimulating formations. Rather than GA, the PSO has no advance administrator, similar to, crossover and change. Speeding up using a shifting term is weighted by outlying subjective numbers being created for expanding speed towards " L_{best} " and " P_{best} " area.

iii. Optimization Procedure:

In the present investigation, the *entropy generation* is selected as an impartial function for the optimization procedure. To diminish the system, another system reliant on coupling of a PSO and

ANN is proposed. This strategy comprises *three phases*; the **primary stage** is to acquire an estimation of entropy generation for numerous limitations of Brownian movement parameter, magnetic parameter, thermophoresis parameter and Brinkman number. In the **secondary stage** a Multi-Layer Perceptron (MLP) neural framework is prepared utilizing Back-Error Propagation (BEP) calculation. In ANN the information sources are the parameters referenced previously. The target production for ANN is relating *entropy generation esteem*. In the **tertiary stage** PSO is deployed to minimize entropy generation values in the biomimetic peristaltic magnetic nanofluid pumping flow. Components and wellness capacity work in the current calculations portray the source of data and the outcomes of correlating of the developed neural system, independently. The essence of this technique is that, the assessment is done once in starting the advance, and hence there is no need to examine the cycle yet again, in light of the way that in the second stage ANN is prepared dependent on examination results of the first stage. Also, the PSO in each stage utilizes the prepared ANN for obtaining robustly the estimations of objective functions.

5. RESULTS AND DISCUSSION:

Extensive numerical computations have been conducted. The robust MATLAB programming [65] has been used to actualize the PSO and ANN algorithms for the present magnetic peristaltic nanofluid duct regime. This section also visualizes selected results for velocity and temperature profiles with variation in Brownian movement parameter N_b , Hartmann number M , thermophoresis parameter N_t , Prandtl number P_r , and thermal Grashof parameter G_{rT} . These are shown in **Figs. 4- 12**. Selected ANN and PSO computational results are shown in **Figs. 13-16**.

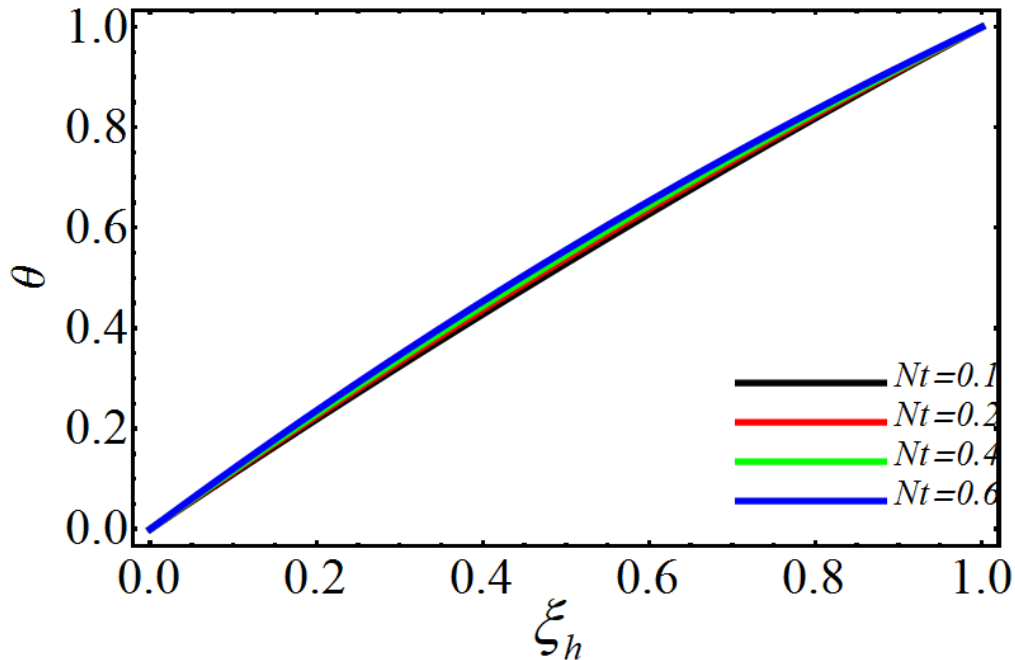


Fig. 4: Thermophoresis parameter N_t impact on θ

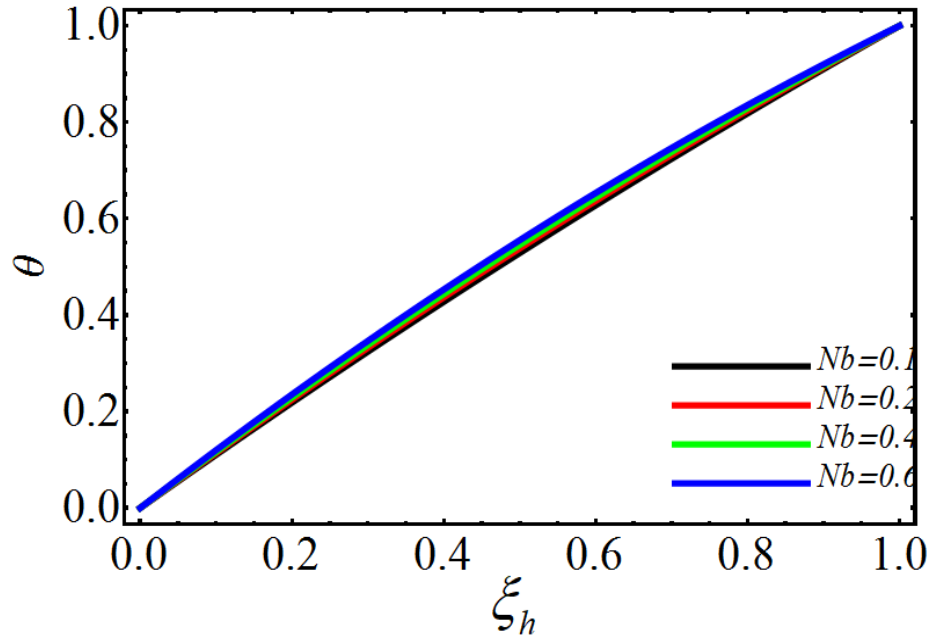


Fig. 5: Brownian motion parameter N_b impact on θ .

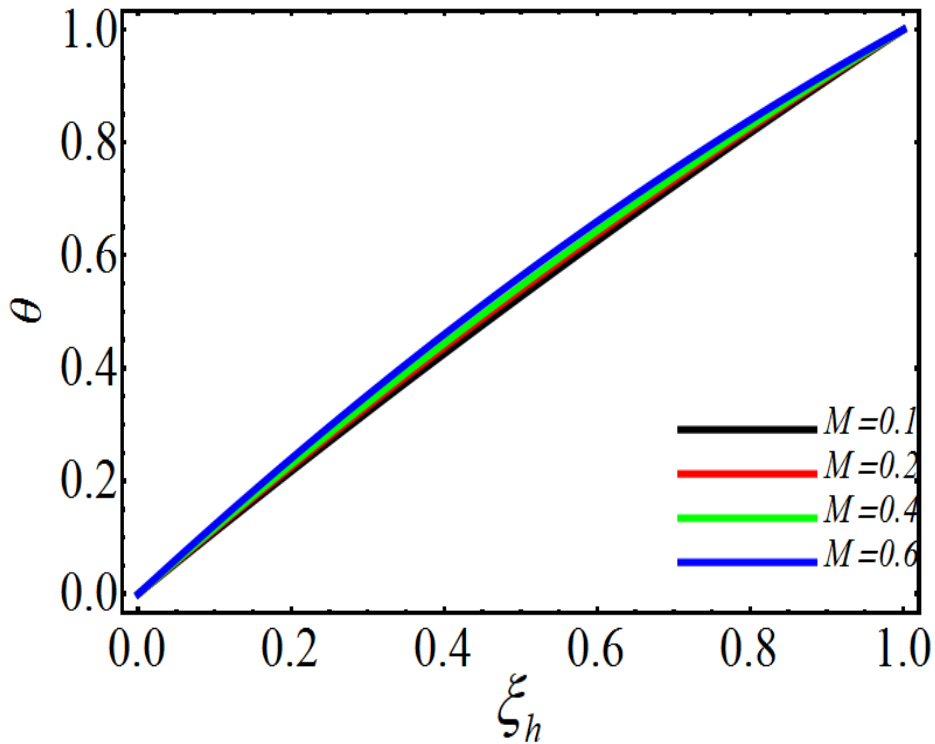


Fig. 6: Magnetic parameter M impact on θ .

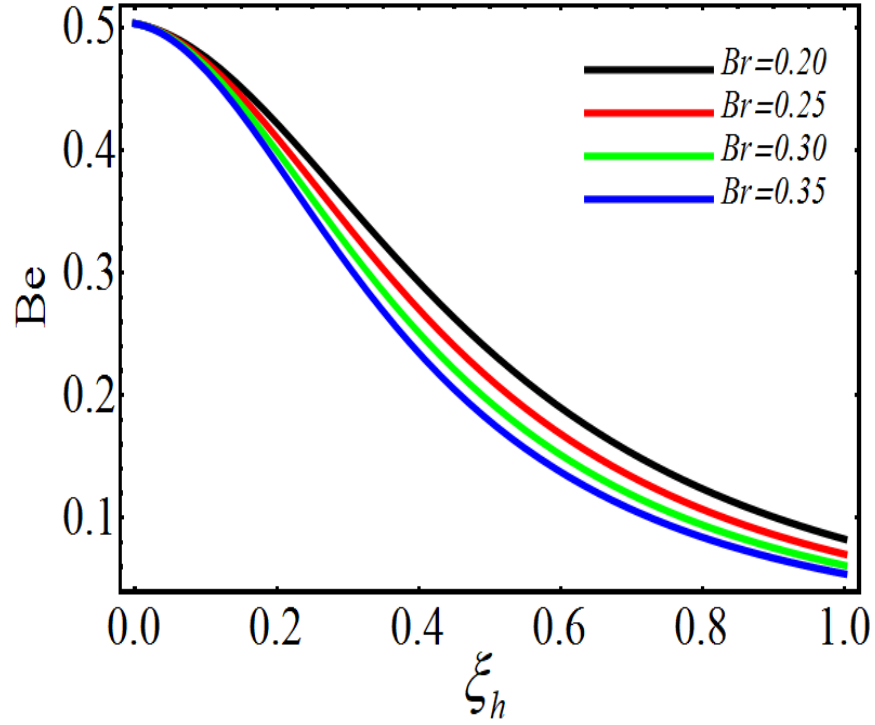


Fig. 7: Impact of Brinkman parameter Br on Be .

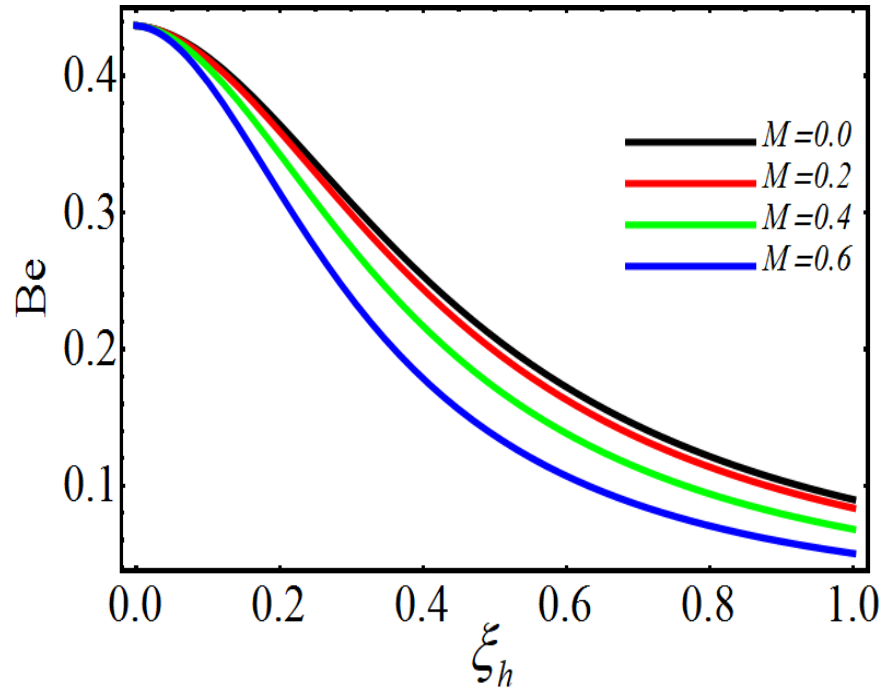


Fig. 8: Magnetic parameter M impact on Be .

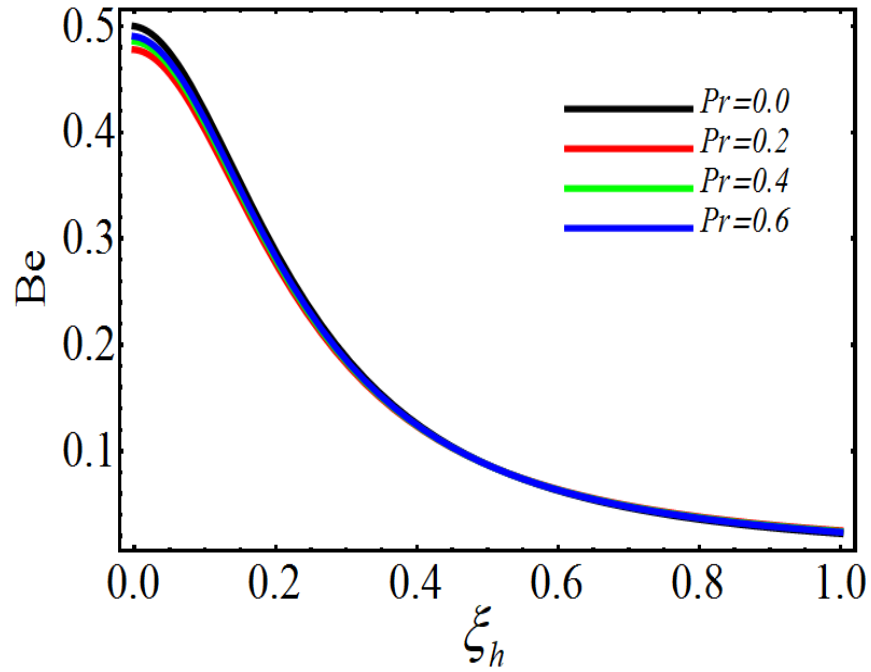


Fig. 9: Prandtl number Pr impact on Be .

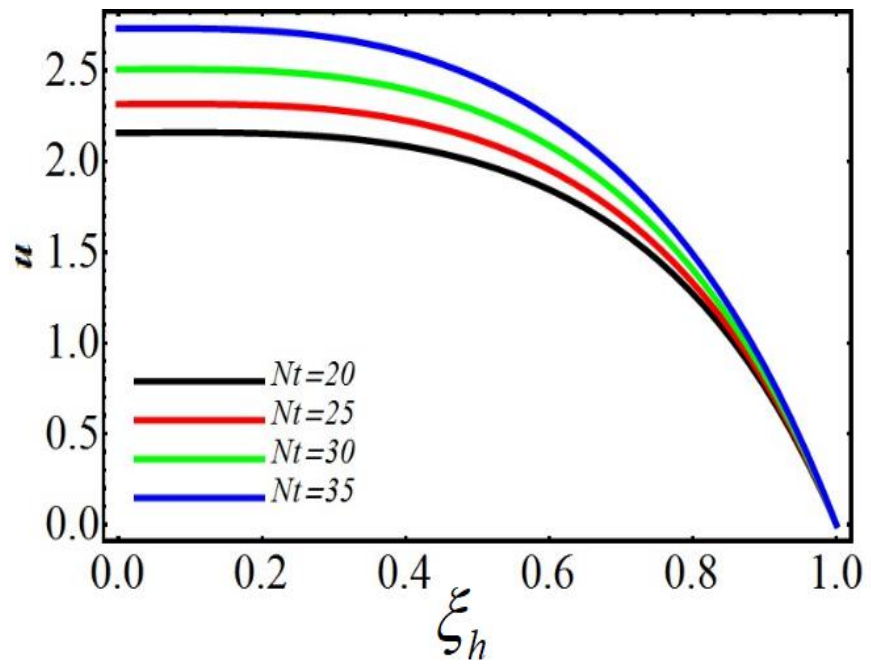


Fig. 10: Thermophoresis parameter N_t impact on u .

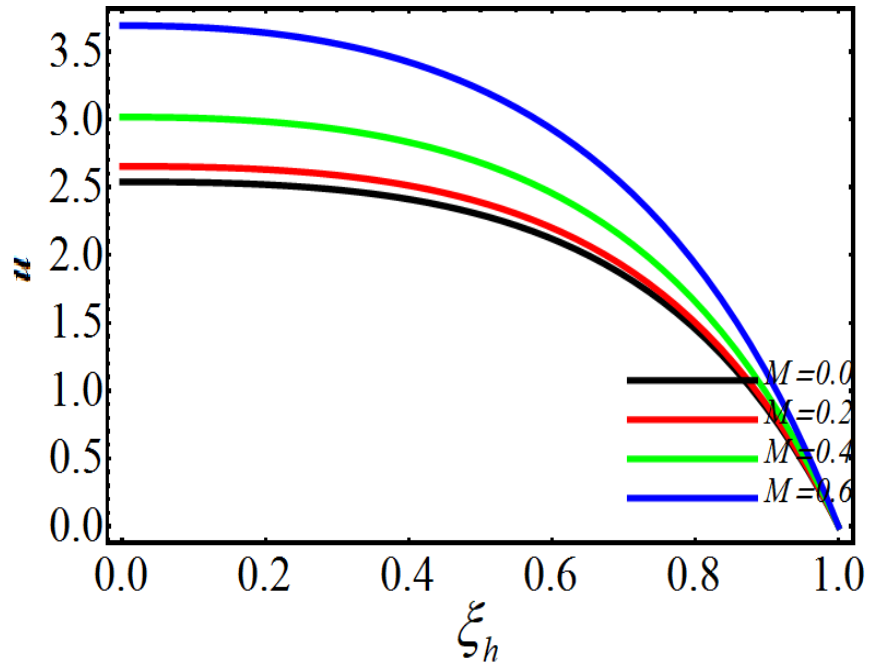


Fig. 11: Magnetic parameter M impact on u .

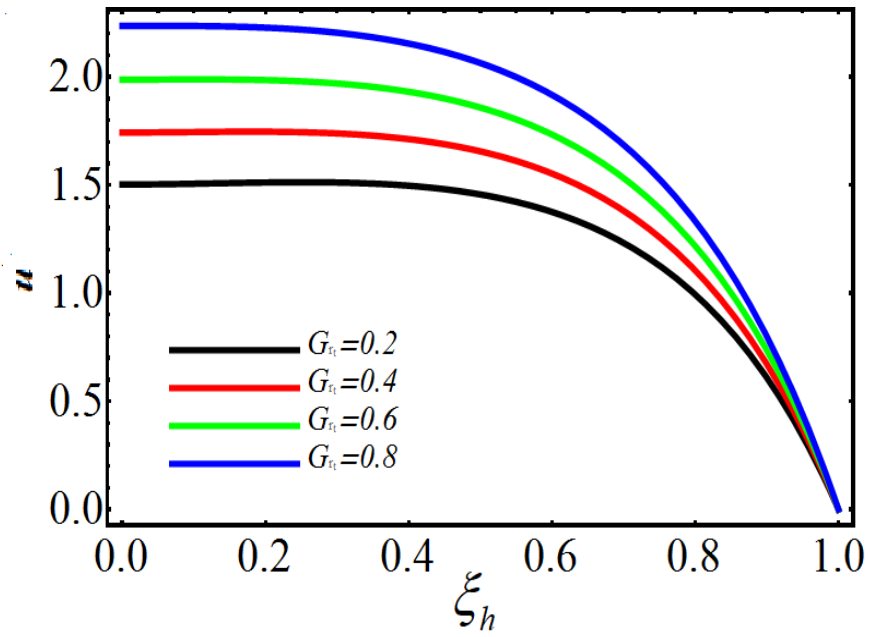


Fig. 12: Thermal Grashof parameter Gr_T impact on u .

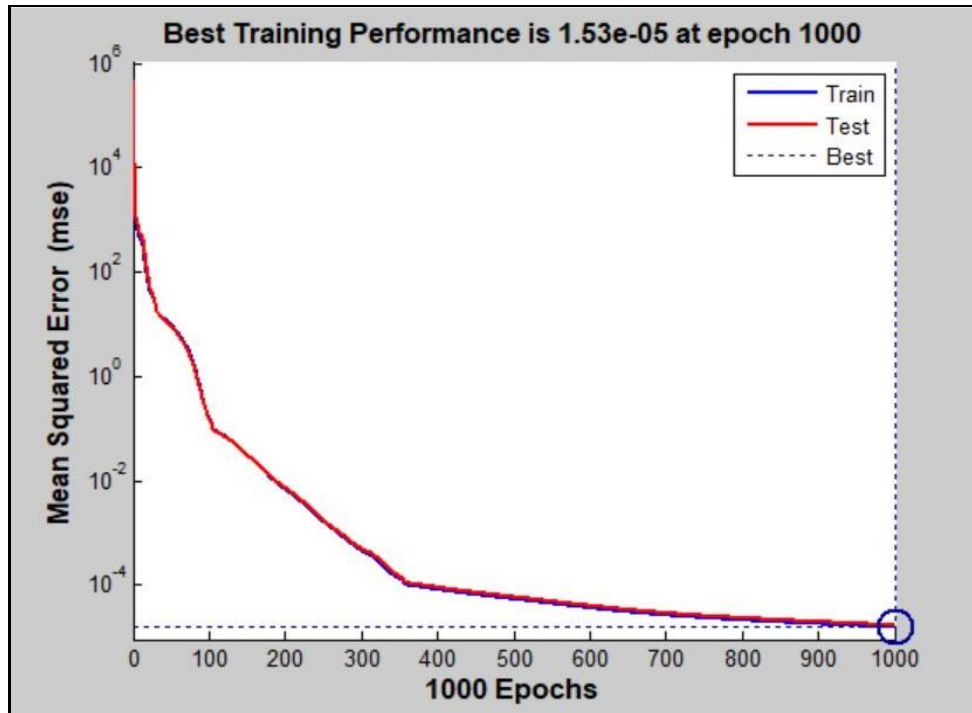


Fig. 13: Training producer of considered MLP neural network.

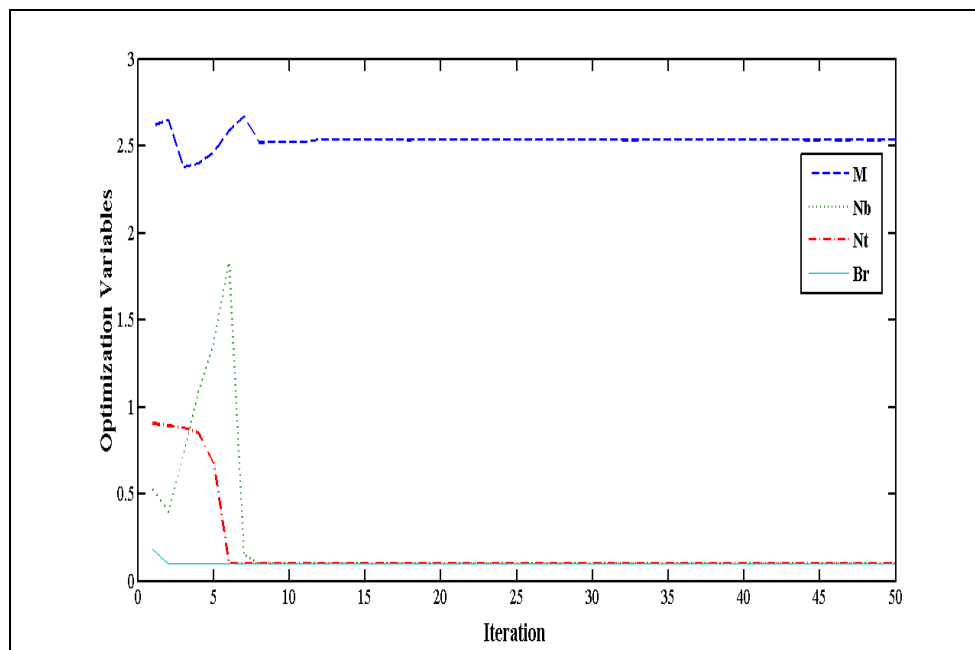


Fig. 14: Variation of the optimization variable during PSO algorithm optimization operation.

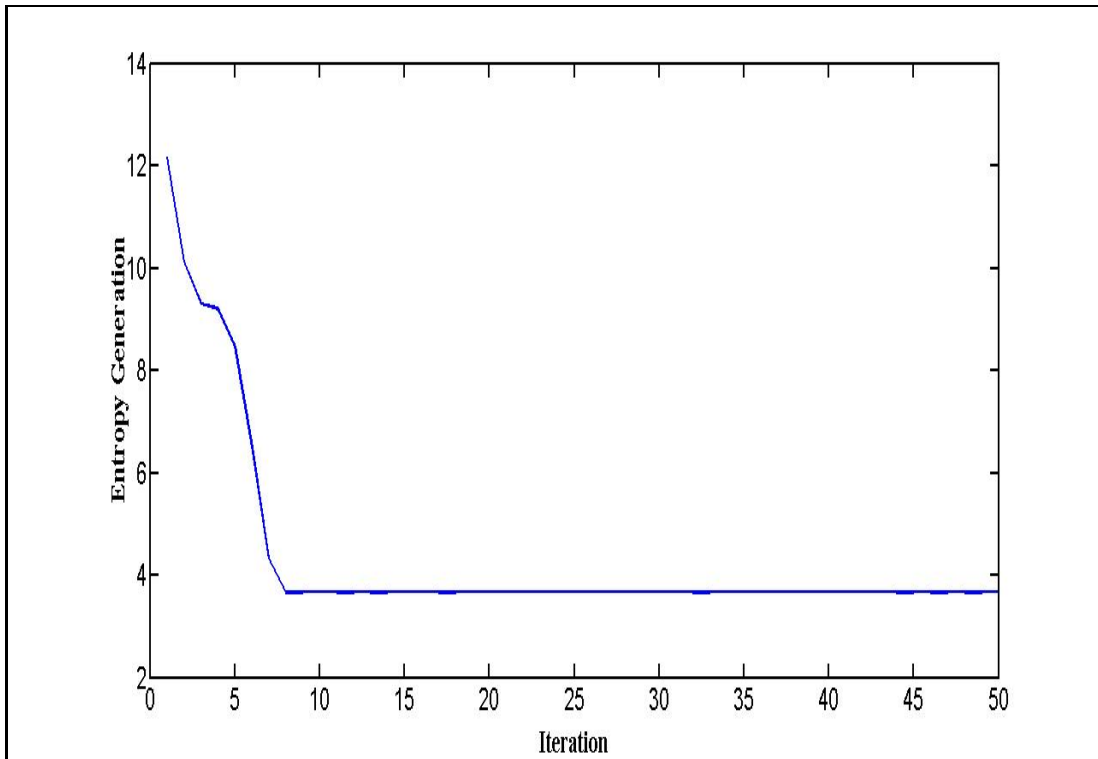


Fig. 15: Entropy generation value minimization method using PSO algorithms.

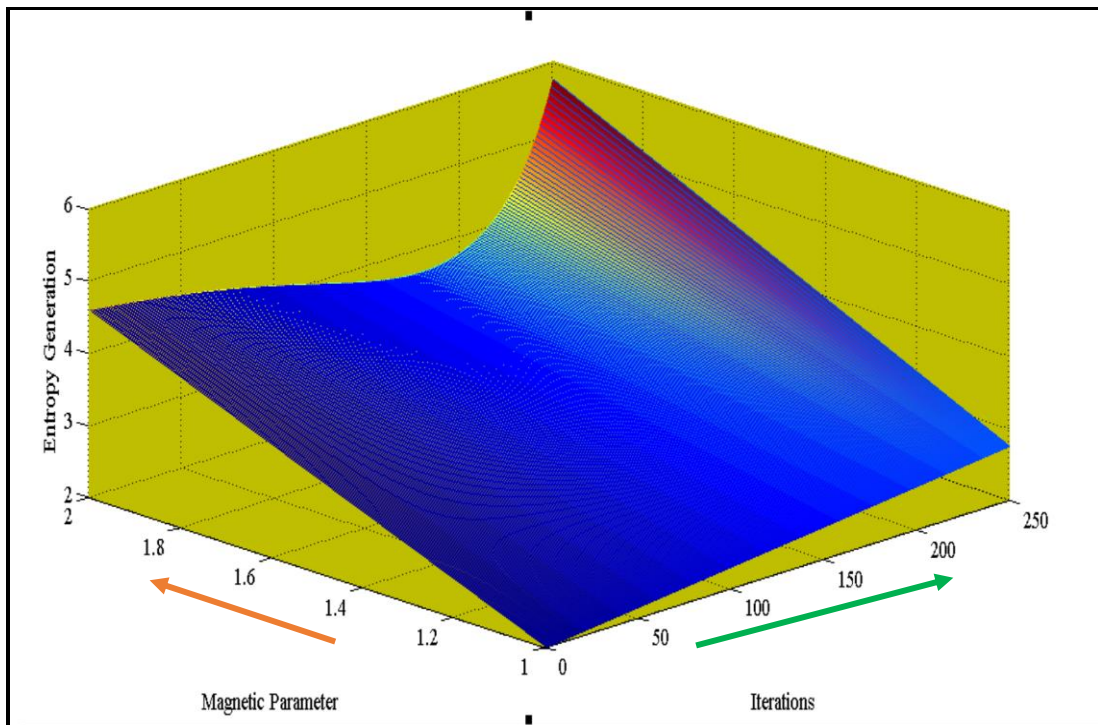


Fig. 16: 3D Continuous entropy layer against magnetic parameter, M

Fig. 4 shows that increasing thermophoresis parameter, N_t significantly elevates temperature profiles. Thermophoretic body force encourages heat (and nanoparticle mass diffusion) with thermal gradient. Monotonic distributions are computed along the channel length i.e. with axial (ξ) coordinate. Thermophoresis is the migration of nano-particles in the direction of a decreasing temperature gradient. Evidently this phenomenon has a potent effect on temperature evolution throughout the channel cross-section. **Fig. 5** also demonstrates that increasing Brownian motion parameter (N_b) increases temperature values (higher N_b corresponds to smaller nanoparticles and encourages thermal and species diffusion to the boundary). Thermal conductivity increases with greater Brownian motion since ballistic collisions in the nanofluid are exacerbated. This heats the peristaltic channel flow regime. The Brownian motion in nanofluid behaves more like a fluid than the conventional solid–fluid mixtures in which relatively larger particles with micrometer or millimeter orders are suspended. The nanofluid is a two-phase fluid in nature and random movement of the suspended nanoparticles increases energy exchange rates in the fluid but depresses concentrations in the flow regime. **Fig. 6** shows that there is an upsurge in the temperature magnitudes with large values of magnetic parameter M . The nanofluid has to expend greater work to drag itself against the action of the retarding magnetic field. This extra work is dissipated as thermal energy which heats the boundary layer. This phenomenon has been identified in many classical viscous magnetohydrodynamics studies including Sutton and Sherman [67]. In all cases $M < 1$ implying that magnetic Lorentz force is less than the viscous hydrodynamic force, as per the definition of Hartmann number, $M = \sqrt{\frac{\sigma}{\mu}} \alpha_0 B_0$.

Figs. (7)-Fig. (9) illustrate the evolution in Bejan number with different values of B_r, M, Pr . Bejan number is the ratio of heat transfer irreversibility to total irreversibility due to heat transfer and fluid friction (viscous effect). With increment in Brinkman number (viscous dissipation) (Fig. 7) there is a significant reduction induced in Bejan number implying that heat transfer irreversibility is suppressed in the system. Also, with greater magnetic field effect there is a substantial depletion (Fig. 8) in Bejan number. With a change in Prandtl number (Fig. 9) there is a slight elevation in Bejan number for lower values of axial coordinate although this largely vanishes subsequently.

Fig. (10) to Fig. (12) display velocity evolution with selected thermophysical parameters. A significant acceleration in axial flow (u) (Fig. 10) is observed with increasing thermophoresis parameter, N_t , with magnitudes maximized at low axial coordinate and minimized at large axial coordinate. Also, a marked acceleration in axial flow (Fig. 11) is generated with increasing magnetic field parameter i.e. Hartmann number, M . This is contrary to conventional findings in magnetohydrodynamics where stronger magnetic fields create retardation in the flow. In the present regime the opposite effect is generated. Fig. 12 shows that greater thermal buoyancy force as simulated via the thermal Grashof number, Gr_T also accelerates the axial flow strongly i.e. increases axial velocity magnitudes. Weaker thermal buoyancy therefore results in considerable axial flow deceleration in the peristaltic regime.

The training arrangement for the considered ANN is conferred in **Fig. 13**. For training 70%

of information is used for alternation, 20% for testing while the remaining 10% for affirming. As clarified in the number the proficient ANN toward the finish of epoch 1000, foresee the estimations of the whole referenced data type, achieving a precision more exact than 10^{-8} . The PSO calculation associated in this study has 100 iterations and the size of population is 10. **Figs. 14 and 15** exhibit the estimations of optimization factors and robustness for the improvement technique produced with several executions of PSO, independently. PSO indicates that the optimum value (minimum) of entropy generation is 3.65 kJ/kg acquired at $M= 3$, $N_b= 0.3$, $N_t = 0.5$ and $B_r = 2$.

The 3D plot of entropy generation alongside the Hartmann (magnetic body force) number) is shown in **Fig 16**. In this figure, it is evident that the entropy generation has a base incentive among upper and lower bounds of the magnetic parameter and is highly sensitive also to iteration count.

6. CONCLUSIONS:

In the present investigation, a mathematical model has been developed for entropy generation in magnetohydrodynamic radiative reactive double diffusive peristaltic pumping of nanofluids in an energy duct containing a porous medium saturated with Williamson non-Newtonian fluid. Due to the complexity of the equations and the multiplicity of the parameters, the optimization process is executed using ANN and PSO. For this purpose, entropy generation is selected as the objective function. The mathematical flow model is transformed with appropriate dimensionless variables and solved as a boundary value problem with the powerful homotopy analysis method (HAM). For minimizing rate of the entropy generation, the effective parameters, namely, Hartmann (magnetic) number, thermophoresis, Brownian motion parameter and Brinkman (dissipation) number are investigated and optimized. The results obtained provide an improved perspective for diminishing the irreversibility causes. The main findings of the present work may be summarized as follows:

- (i) The PSO algorithm determines the optimum value (minimum) of entropy generation as 3.65 kJ/kg acquired at $M= 3$, $N_b= 0.3$, $N_t = 0.5$ and $B_r = 2$. This is very important to find out the sensitivity of each parameter in entropy generation.
- (ii) Magnetic Lorentz force is less than the viscous hydrodynamic force due to which it is concluded that entropy generation is strongly dependent on both magnetic parameter and iteration count.
- (iii) Bejan number is depressed with greater Brinkman number (viscous dissipation) i.e. heat transfer irreversibility is suppressed in the system.
- (iv) Bejan number is also depleted with greater Hartmann (magnetic) number.
- (v) Increasing thermophoresis parameter and thermal Grashof number, both accelerate the axial flow.
- (vi) Increasing Brownian motion parameter, thermophoresis parameter and Hartmann (magnetic) number all elevate temperatures in the peristaltic channel regime.

The current study has demonstrated the excellent facility of PSO/ANN algorithms in

thermodynamic optimization of bioinspired electromagnetic nanofluid flows. Future studies may consider combined electrical and magnetic field effects and will be communicated imminently.

Conflicts of Interest: The authors declare no conflict of interest.

REFERENCES

- [1] A. Arikoglu, I. Ozkol, G. Komurgoz, Effect of slip on entropy generation in a single rotating disk in MHD flow, *Applied Energy*. 85 (2008) 1225-1236.
- [2] M. M. Rashidi, M. Ali, N. Freidoonimehr, F. Nazari, Parametric analysis and optimization of entropy generation in unsteady MHD flow over a stretching rotating disk using artificial neural network and particle swarm optimization algorithm, *Energy*. 55 (2013) 497-510.
- [3] J. V. Ramana Murthy, J. Srinivas and **O. Anwar Bég**, Entropy generation analysis of radiative heat transfer effects on channel flow of two immiscible couple stress fluids, *J. Brazilian Soc. Mech Sci. Eng*, 39, 2191–2202 (2017).
- [4] D. Tarlet, Y. Fan, S. Roux, L. Luo, Entropy generation analysis of a mini heat exchanger for heat transfer intensification, *Experimental Thermal and Fluid Science*. 53 (2014) 119-126.
- [5] M. Sheikholeslami, R. Ellahi, H. R. Ashorynejad, G. Domairry, T. Hayat, Effects of heat transfer in flow of nanofluids over a permeable stretching wall in a porous medium, *J. Computational and Theoretical Nanoscience*. 11 (2014) 486-496.
- [6] A. Bejan, Second-law analysis in heat transfer and thermal design. *Advances in Heat Transfer*, 14, (1982) 151-58.
- [7] S. Aïboud, S. Saouli, Second law analysis of viscoelastic fluid over a stretching sheet subject to a transverse magnetic field with heat and mass transfer, *Entropy*. 12 (2010) 1867-1884.
- [8] H. F. Oztop, K. Al-Salem, A review on entropy generation in natural and mixed convection heat transfer for energy systems, *Renewable and Sustainable Energy Reviews*. 16 (2012) 911-920.
- [9] M.I. Afridi, M. Qasim, Entropy generation and heat transfer in boundary layer flow over a thin needle moving in a parallel stream in the presence of nonlinear Rosseland radiation, *Int. J. Therm. Sci.* 123 (2018) 117–128.
- [10] A. López, G. Ibáñez, J. Pantoja, J. Moreira, O. Lastres, Entropy generation analysis of MHD nanofluid flow in a porous vertical microchannel with nonlinear thermal radiation, slip flow and convective-radiative boundary conditions, *Int. J. Heat Mass Transf.* 107 (2017) 982–994.
- [11] S. Baag, S.R. Mishra, G.C. Dash, M.R. Acharya, Entropy generation analysis for viscoelastic MHD flow over a stretching sheet embedded in a porous medium, *Ain Shams Eng. J.* 8 (2017) 623–632.
- [12] Y. Liu, Y. Jian, W. Tan, Entropy generation of electromagnetohydrodynamic (EMHD) flow in a curved rectangular microchannel, *Int. J. Heat Mass Transf.* 127 (2018) 901–913.
- [13] Nakhchi, M. E., & Rahmati, M. T. (2020). Entropy generation of turbulent Cu–water nanofluid flows inside thermal systems equipped with transverse-cut twisted turbulators. *Journal of Thermal Analysis and Calorimetry*, 1-10.

- [14] Nakhchi, M. E., Esfahani, J. A., & Kim, K. C. (2020). Numerical study of turbulent flow inside heat exchangers using perforated louvered strip inserts. *International Journal of Heat and Mass Transfer*, 148, 119143.
- [15] Nakhchi, M. E., & Esfahani, J. A. (2020). Numerical investigation of heat transfer enhancement inside heat exchanger tubes fitted with perforated hollow cylinders. *International Journal of Thermal Sciences*, 147, 106153.
- [16] N. Hidouri *et al.*, Effects of radiation heat transfer on entropy generation in thermosolutal convection in a square cavity subjected to a magnetic field, *Entropy* (2011), 13(12), 1992-2012.
- [17] T. Wenterodt *et al.*, Second law analysis for sustainable heat and energy transfer: The entropic potential concept, *Applied Energy*, 1391 (2015) 376-383.
- [18] Kalogirou SA. Artificial intelligence for the modeling and control of combustion processes: a review. *Progress in Energy and Combustion Science*. 29(6) (2003) 515-66.
- [19] Deh Kiani MK, Ghobadian B, Tavakoli T, Nikbakht AM, Najafi G. Application of artificial neural networks for the prediction of performance and exhaust emissions in SI engine using ethanol-gasoline blends. *Energy*. 35(1) (2010) 65-9.
- [20] Gandhidasan P, Mohandes MA. Artificial neural network analysis of liquid desiccant dehumidification system. *Energy*. 36(2) (2011) 1180-6.
- [21] Smrekar J, Assadi M, Fast M, Ku-strin I, De S, Development of artificial neural network model for a coal-fired boiler using real plant data. *Energy*. 34(2) (2009) 144-52.
- [22] Atashkari K, Nariman-Zadeh N, Pilechi A, Jamali A, Yao X, Thermodynamic Pareto optimization of turbojet engines using multi-objective genetic algorithms. *International Journal of Thermal Sciences*. 44(11) (2005) 1061-71.
- [23] Mohagheghi M, Shayegan J, Thermodynamic optimization of design variables and heat exchangers layout in HRSGs for CCGT, using genetic algorithm. *Applied Thermal Engineering*. 29(23) (2011) 290-299.
- [24] Rashidi, M. M., **Bég, O. Anwar**, Parsa, A. B., & Nazari, F, Analysis and optimization of a transcritical power cycle with regenerator using artificial neural networks and genetic algorithms. *Proc. IMechE- Part A: Journal of Power and Energy*. 225(6) (2011) 701-717.
- [25] Rao RV, Patel VK, Thermodynamic optimization of cross flow plate-fin heat exchanger using a particle swarm optimization algorithm. *International Journal of Thermal Sciences*. 49 (9) (2010) 1712-1721.
- [26] Rashidi MM, Galanis N, Nazari F, Basiri Parsa A, Shamekhi L, Parametric analysis and optimization of regenerative Clausius and organic Rankine cycles with two feedwater heaters using artificial bees' colony and artificial neural network. *Energy*. 36(9) (2011) 5728-5740.
- [27] Zhang Z, Zeng Y, Kusiak A, Minimizing pump energy in a wastewater processing plant. *Energy*. 47(1) (2012) 505-514.
- [28] S. Pu *et al.*, Bioinspired sweating with temperature sensitive hydrogel to passively dissipate heat from high-end wearable electronics, *Energy Conversion and Management*, 18015 (2019) 747-756.

- [29] R. Salazar and A. Abdelkefi, Nonlinear analysis of a piezoelectric energy harvester in body undulatory caudal fin aquatic unmanned vehicles, *Applied Energy*, 2631 (2020) Article 114627.
- [30] N. Athanopoulos and N. J. Siakavellas, Programmable thermal emissivity structures based on bioinspired self-shape materials *Scientific Reports*, 5, Article number: 17682 (2015).
- [31] R. Gulfam, P. Zhang, Power generation and longevity improvement of renewable energy systems via slippery surfaces – A review, *Renewable Energy*, 143 (2019) 922-938.
- [32] Y.C. Fung, *Biomechanics: Motion, Flow, Stress and Growth*, MacGraw-Hill, New York (1990).
- [33] V. K. Narla, Dharmendra Tripathi, **O. Anwar Bég**, Analysis of entropy generation in biomimetic electroosmotic nanofluid pumping through a curved channel with joule dissipation, *Thermal Science and Engineering Progress*, 151 (2020) Article 100424.
- [34] M. M. Bhatti, A. Zeeshan, N. Ijaz, **O. Anwar Bég** and **A. Kadir**, Mathematical modelling of nonlinear thermal radiation effects on EMHD peristaltic pumping of viscoelastic dusty fluid through a porous medium channel, *Engineering Science and Technology*, 20 (3), 1129-1139 (2017).
- [35] M. M. Bhatti, A. Zeeshan, R. Ellahi, **O. Anwar Bég** and **A. Kadir**, Effects of coagulation on the two-phase peristaltic pumping of magnetized Prandtl biofluid through an endoscopic annular geometry containing a porous medium, *Chinese J. Physics*. 58, 222-234 (2019).
- [36] N. Ali, S. Hussain, K. Ullah, **O. Anwar Bég**, Mathematical modelling of Ellis/Newtonian two-fluid electro-osmotic peristaltic pumping in an axisymmetric tube, *European Physical Journal Plus*, 134, 1-18 (2019).
- [37] D. Tripathi, A. Yadav and **O. Anwar Bég**, Electro-kinetically driven peristaltic transport of viscoelastic physiological fluids through a finite length capillary: *mathematical modelling*, *Mathematical Biosciences*, 283, 155-168 (2017).
- [38] Sara I. Abdelsalam, M. M. Bhatti, A. Zeeshan, A. Riaz and **O. Anwar Bég**, Metachronal propulsion of magnetized particle-fluid suspension in a ciliated channel with heat and mass transfer, *Physica Scripta*, 94, 115301 (13pp) (2019).
- [39] J. Prakash, D. Tripathi, **O. Anwar Bég**, Comparative study of hybrid nanofluid performance in microchannel slip flow induced by electroosmosis and peristalsis, *Applied Nanoscience* (2020). (14 pages). doi.org/10.1007/s13204-020-01286-1
- [40] C.T. Weng *et al.*, Overview of porous media/metal foam application in fuel cells and solar power systems, *Renewable and Sustainable Energy Reviews*, 96 (2018) 181-197.
- [41] Alkam, M.K. and Al-Nimr, M.A. Solar collectors with tubes partially filled with porous substrate. *ASME J. Solar Energy Eng.* 121 (1999) 20-24.
- [42] M. A. El Tawil, M. H. Kamel, MHD flow under stochastic porous media, *Energy Conversion and Management*, 35 (1994) 991-997.
- [43] M. H. Kamel, Unsteady MHD convection through porous medium with combined heat and mass transfer with heat source/sink, *Energy Conversion and Management*, 42 (2001) 393-405.

- [44] J. Zueco, P. Eguía, E. Granada, J. L. Míguez, **O. Anwar Bég**, An electrical network for the numerical solution of transient MHD Couette flow of a dusty fluid: Effects of variable properties and Hall current, *Int. Comm. Heat Mass Transfer*, 37, 1432–1439 (2010).
- [45] **O. Anwar Bég**, Sandile S. Motsa, A. Kadir, Tasveer A. Bég and M.N. Islam, Spectral quasilinear numerical simulation of micropolar convective wall plumes in high permeability porous media, *J. Engineering Thermophysics*, 25 (4) 1–24 (2016).
- [46] J.W. Hoyt, Some applications of non-Newtonian fluid flow, D.A. Siginer, D. De Kee, R.P. Chhabra (Eds), *Advances in the Flow and Rheology of Non-Newtonian Fluids, Rheology Series*, 8 (1999) 797-826.
- [47] R. Nebbali and K.Bouhadef, Non-Newtonian fluid flow in plane channels: Heat transfer enhancement using porous blocks, *Int. J. Thermal Sciences*, 50 (2011) 1984-1995.
- [48] R.V. Williamson, The flow of pseudoplastic materials. *Ind Eng Chem*, 21 (1929) 1108–1111.
- [49] Cramer SD, Marchello JM. Numerical evaluation of models describing non-Newtonian behavior. *AIChE J.*, 14 (1968) 980–983.
- [50] T. Hayat, Peristaltic flow of Williamson fluid in a convected walls channel with Soret and Dufour effects, *International Journal of Biomathematics*, Vol. 09 (2016), 1650012.
- [51] **O. Anwar Bég et al.** Multi-Step DTM simulation of magneto-peristaltic flow of a conducting Williamson viscoelastic fluid, *Int. J. Applied Mathematics Mechanics*, 9 (12): 22-40 (2013).
- [52] Liao, S.J. (2003). *Beyond Perturbation: Introduction to the Homotopy Analysis Method*, Boca Raton: Chapman & Hall/ CRC Press, Florida, USA.
- [53] Turkyilmazoglu, M. (2012). An effective approach for approximate analytical solutions of the damped Duffing equation. *Physica Scripta*, 86(1), 015301.
- [54] Turkyilmazoglu, M. (2019). Latitudinally deforming rotating sphere. *Applied Mathematical Modelling*, 71, 1-11.
- [55] Turkyilmazoglu, M. (2018). Convergence accelerating in the homotopy analysis method: a new approach. *Adv Appl Math Mech*, 10(4), 925-947.
- [56] Turkyilmazoglu, M. (2011). An optimal analytic approximate solution for the limit cycle of Duffing–van der Pol equation. *Journal of applied mechanics*, 78(2).
- [57] Turkyilmazoglu, M. (2020). Single phase nanofluids in fluid mechanics and their hydrodynamic linear stability analysis. *Computer Methods and Programs in Biomedicine*, 187, 105171.
- [58] J. Srinivas and **O. Anwar Bég**, Homotopy study of entropy generation in magnetized micropolar flow in a vertical parallel plate channel with buoyancy effect, *Heat Transfer Research*, 49(6): 529–553 (2018).
- [59] A. K. Ray, B Vasu, **O. Anwar Bég**, R. S R Gorla and P. V. S. N. Murthy, Homotopy semi-numerical modelling of non-Newtonian nanofluid transport external to multiple geometries using

- a revised Buongiorno model, *Inventions*, 4, 54, 1-27 (2019). doi:10.3390/inventions4040054 (2019).
- [60] McClelland JL, Rumelhart DE, P.D.P.R. Group. Parallel distributed processing. In: *Psychological and Biological Models*. 2 (1987).
- [61] Foresee, F. D., & Hagan, M. T, Gauss-Newton approximation to Bayesian learning. In *Proceedings of International Conference on Neural Networks*. 3 (1997) 1930-1935.
- [62] MacKay, D. J, Bayesian interpolation. *Neural Computation*. 4(3) (1992) 415-447.
- [63] Kennedy, J.; Eberhart, R.C. (2001). *Swarm Intelligence*. Morgan Kaufmann, USA.
- [64] Poli, R., J. Kennedy, and T. Blackwell. Particle Swarm Optimization, *Swarm Intelligence*. 1 (2007) 33-57.
- [65] *MATLAB*, The MathWorks Inc., Boston, USA, Version 2010 a.
- [66] V. K. Narla, D. Tripathi, **O. Anwar Bég** and **A. Kadir**, Modelling transient magnetohydrodynamic peristaltic pumping of electroconductive viscoelastic fluids through a deformable curved channel, *J. Engineering Mathematics*, 111, 127–143 (2018).
- [67] Sutton, George W., and Sherman, Arthur, *Engineering Magnetohydrodynamics*, McGraw-Hill Book Company, New York, USA (1965).